Article

Journal of
Biomedical Nanotechnology
Vol. 15, 507–517, 2019
www.aspbs.com/jbn

Helicobacter pylori Ribosomal Protein-A2 Peptide/ Silk Fibroin Nanofibrous Composites as Potential Wound Dressing

Dongdong Zhang[1], Linpeng Fan[2], Linlin Ma[1], Junqiu Liu[3], Kai Zhou[1], Xinran Song[1], Meiqi Sun[1], Xiumei Mo[1], Chuanglong He[1], Yuxin Chen[4,*], and Hongsheng Wang[1,*]

[1] *Key Laboratory of Science and Technology of Eco-Textiles, Ministry of Education, College of Chemistry, Chemical Engineering and Biotechnology, Donghua University, Shanghai 201620, China*
[2] *Institute for Frontier Materials, Deakin University, Geelong, Victoria 3216, Australia*
[3] *Laboratory of Medicinal Plant Biotechnology, College of Pharmaceutical Sciences, Zhejiang Chinese Medical University, Hangzhou, 310053, China*
[4] *Jiangsu ProteLight Pharmaceutical & Biotechnology Co., Ltd., Jiangyin 214437, China*

Although different kinds of antibacterial formulas have been explored against bacterial infections, the development of both biocompatible and efficiently antibacterial matrices is still a challenge. In this study, we report a novel HPRP-A2 antimicrobial peptide/silk fibroin (SF) composite nanofibrous matrix fabricated by an all-aqueous electrospinning process (HPRP-A2 is an antibacterial peptide originated from *Helicobacter pylori*). The HPRP-A2/SF composite nanofibers had a round and smooth morphology. The incorporation of HPRP-A2 had little influence on both the morphology and biocompatibility of the SF nanofibers. Interestingly, the composite nanofibrous matrices showed an impressive antimicrobial activity against both Gram-positive and Gram-negative bacteria. Furthermore, the HPRP-A2/SF composite nanofibers showed excellent performance on accelerating healing of wound according to the data of animal experiment. Considering the facile and all-aqueous process, the HPRP-A2/SF composite nanofibrous matrices could be a promising candidate for antibacterial or wound management applications.

KEYWORDS: *Silk Fibroin, Antibacterial Peptide, Green Electrospinning, Nanofiber, Wound Dressings, Antibacterial Management.*

INTRODUCTION

Skin is the most important and largest barrier against pathogen invasion.[1] However, the skin wounds are often exposed to various bacterial infections due to a lack of appropriate treatment, leading to a prolonged inflammation and thus delaying wound healing.[2] Therefore, the treatment of chronic non-healing wounds is still a challenge for doctors and the costs of healthcare.[3] Wound dressings help to prevent dehydration and reduce the risk of bacterial infections. An ideal wound dressing should be able to inhibit the bacteria, maintain moisture and pH, and thus accelerate the wound healing process.[4] Over the past decades, a wide variety of wound dressing materials have been developed from natural and synthetic polymers, such as cotton, poly(ε-caprolactone), polyurethane, cellulose acetate, chitosan, alginate and collagen.[5–8] However, the performance of most of these products is unsatisfactory due to their poor antibacterial activities or biocompatibility, leading to a prolonged healing or large scars.[9] In order to prevent the infection of bacteria, many antibacterial drugs such as antibiotics have been used for wound care.[10] However, the wide use of traditional antibiotics has led to an emergence of resistant bacteria in hospitals and communities, which has become a serious threat to human health.[11,12] While some alternative materials have either a considerable cell toxicity (such as silver ions), or a low antibacterial efficacy (such as chitosan).[13,14] In recent years, the antimicrobial peptides (AMPs), whether native or artificial products, have attracted great attention for their remarkable antibacterial

*Authors to whom correspondence should be addressed.
Emails: chen.yuxin@protelight.com, whs@dhu.edu.cn
Received: 25 September 2018
Accepted: 8 November 2018

properties with a low drug resistance.[15,16] Originated from mammals, fishes or amphibians, AMPs play a key role in protecting their host from bacteria as a part of the innate immune system.[17,18] AMPs are generally composed of 5–100 amino acid residues and are often cationic due to the sufficiency of lysine, arginine and histidine amino acids. With unique amino sequences, AMPs can insert into the cell membrane of bacteria and subsequently kill them by disrupting their membrane integrity.[10,19] *Helicobacter pylori* ribosomal protein A1 (HPRP-A1), a cationic and amphipathic AMP with 15 L-amino acid residues, is derived from the N-terminus of ribosomal protein L1 of *Helicobacter pylori*.[20,21] HPRP-A2, obtained by transforming HPRP-A1 into the whole D-peptide, has the similar antimicrobial activity but much higher stability than HPRP-A1.[12,21] Thus, HPRP-A2 is a better antibacterial additive for various biomaterials.

Silk fibroin (SF) is a promising biomaterial due to its excellent biocompatibility, tunable structure and oxygen permeability.[18,22] Specifically, SF nanofibrous matrices have attracted lots of attention for its biomimetic structure to the native extracellular matrix (ECM), with high surface area and porosity.[22,23] Previous studies have demonstrated the outstanding performances of SF nanofibrous matrices on skin care.[2,25–28] and wound healing.[22] However, the antibacterial activity of neat SF nanofibrous matrices is weak. We previously reported the great beneficial of honey-loaded SF matrices to wound healing,[2] which indicated that the combination of SF and antibacterial substance is an effective way to construct wound dressings.

Based on the previous studies, this work is to develop a biocompatible and antibacterial nanofibrous wound dressings by a combination of HPRP-A2 and silk (Scheme 1) fibroin via a green electrospinning process developed by our team.[24–28] The physical and chemical properties, cytocompatibility as well as antibacterial activity of nanofibrous matrices were investigated with scanning electronic microscopy (SEM), X-ray diffraction (XRD), attenuated total reflection-fourier transform infrared spectroscopy (ATR-FTIR), cell viability and bacteriostatic assays.

EXPERIMENTAL REAGENTS AND INSTRUMENTS

Cocoons of *B. mori silkworm* were purchased from Hu zhou Silk Co. (China). HPRP-A2 were kindly provided by Jiangsu ProteLight Pharmaceutical and Biotechnology Co., Ltd. (China). Poly(ethylene oxide) with an average molecular weight of 9×10^5 g/mol (Aldrich) was used in the blends. L929 cells were provided by Institute of Biochemistry and Cell Biology (Chinese Academy of Sciences, China). *Escherichia coli*, *Staphylococcus aurous*, *Pseudomonas aeruginosa* and *Staphylococcus epidermidis* were purchased from Shanghai Shifeng Biological Technology Co. (China). ICR mice, 6–8 weeks old, purchased from Shanghai SLAC Laboratory Animal Co., Ltd. (China). The commercial product wound plaster was purchased from Qingdao Hainuo Biological Engineering CO. (China). All other chemicals were analytical grade or higher and used as received. Ultrapure water was used throughout the whole study.

Preparation of Regenerated SF

The regenerated SF was prepared using a modified method described in our previous report.[24–28] Briefly, raw silkworm cocoons were boiled in 0.5% (wt/v) Na_2CO_3 aqueous solution for 45 min to remove the sericin protein, and then the residual sericin was removed by rinsing with warm ultrapure water. The sericin-free silk fibers were dissolved in 9.3 M LiBr for 1 hour to obtain a homogeneous solution. After dialysis with cellulose dialysis tubing (MWCO = 14000) at room temperature for 72 h against water, the resulting solution was filtered and lyophilized to obtain regenerated SF sponges.

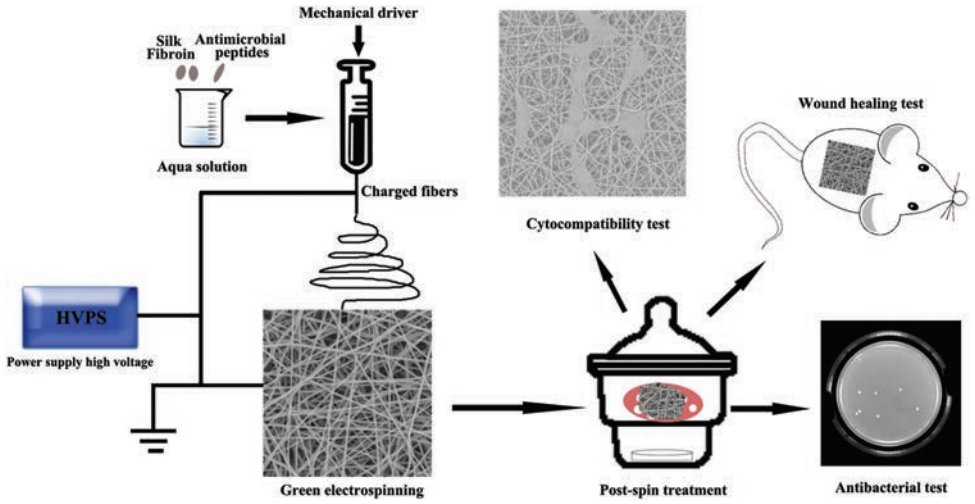

Scheme 1. **Illustration of the fabrication and characterization of the nanofibrous composites.**

Fabrication of HPRP-A2-Loaded SF Nanofibrous Matrices

For electrospinning, 1.0 g of SF, 0.1 g of PEO and certain amounts of HPRP-A2 were dissolved in 5 mL ultrapure water to obtain blend solution containing different amounts of HPRP-A2 (0, 0.002% (w/v), 0.004% (w/v), 0.01% (w/v), respectively). Then, this solution was transferred to a syringe and electrospun onto aluminum foil with a rate of 1.0 mL/h under 12 Kv of voltage. After drying, as-spun nanofibrous matrices were stored in a desiccator for further use.

Surface Morphology of Nanofibrous Matrices

Surface morphology of the samples was observed by SEM (JEOL, JSM-5600, Japan) after sputter-coating by gold at 7 mA for 45 s. Mean fiber diameter was determined by counting 100 random points on SEM images using a Image-J software (National Institutes of Health, USA).

ATR-FTIR Analysis

The samples were dried in a vacuum drying oven before analysis. In order to understand the interactions between SF and the antibacterial peptide, the ATR infrared spectroscopy of matrices was scanned from 400 cm^{-1} to 4000 cm^{-1} using an ATR-FTIR spectrometer (Avatar 380, USA).

XRD Analysis

The samples were detected using a D/Max-2550PC diffractometer (Rigaku, Japan) to determine their structure. The measurement parameters were set to Cu Ka1, 40 kV and 300 mA. The 2θ range of XRD data was 5°–60°.

Cytocompatibility Evaluation

Cell Culture

L929 cells were initially cultured in DMEM (high glucose) medium (HyClone) supplemented with 10% FBS (Gibco, Invitrogen), 100 U/mL penicillin and 100 mg/ml streptomycin (Gibco, Invitrogen) in a humidified incubator of 5% CO_2 at 37 °C. The electrospun nanofibrous matrices were collected on cover slips (14 mm in diameter) for cell culture. After treated with 75% (v/v) ethanol vapor, the matrix-deposited cover slips were fixed with stainless steel rings and soaked in cell culture medium before cell seeding and fiber-free cover slips as controls. L929 cells were seeded on the nanofibrous matrices at a density of 1×10^4 cells/well. The cell culture medium was replaced with fresh medium for every 2 days.

Cell Viability Assay

The viability of L929 cells on the nanofibrous matrices was assessed using MTT assay. After 1, 3 and 5 days of incubation, the matrices were rinsed three times with PBS following medium being removed. Thereafter, each well was supplemented with 400 μL of serum-free DMEM containing 0.5 mg/mL MTT (Sigma-Aldrich) for 4 hours at 37 °C. After 4 hours of incubation, the medium was removed and the formed formazan was dissolved in 400 μL of dimethyl sulfoxide. Then, 100 μL of the solution was withdrawn to 96 well plates to measure the absorption at 492 nm using a microplate reader (Thermo, USA), and the background value of cell-unseeded nanofibrous matrices or cover slips was taken out correspondingly.

To observe the morphology of cells grown on the matrices, the medium was removed after 3 days incubation, and 4% paraformaldehyde was used to fix the cells at 4 °C for 4 hours and the cells were rinsed with PBS three times. The samples were then divided into two parts and treated respectively as follows: for part I, the samples were dehydrated with gradient concentrations of ethanol solutions and dried in a vacuum drying oven. Subsequently, the samples were sputter-coated with gold and observed using SEM (JEOL, JSM-5600, Japan); for part II, the samples were successively treated with 0.1% (v/v) Trion X-100 and 2% (w/v) bovine serum albumin for 5 minutes and 30 minutes, respectively, and then stained with DAPI for 15 minutes and Alexa Fluor® 568 phalloidin for 30 minutes. Finally, the cells were observed with a fluorescence microscope.

Antibacterial Activity Measurement

Antimicrobial activity of the HPRP-A2/SF nanofibrous matrices was measured based on the AATCC Quantitative Test Method 100-1999 against *Escherichia coli* (*E. coli*), *Pseudomonas aeruginosa* (*P. aeruginosa*), *Staphylococcus aureus* (*S. aureus*) and *Staphylococcus epidermidis* (*S. epidermidis*). *E. coli*, *P. aeruginosa*, *S. aureus* and *S. epidermidis* were cultured in medium for 18–20 h in a shake table at 37 °C with a rotating speed of 100 r/min. Then, the bacterial suspension was centrifuged at 3000 rpm for 5 minutes, and the bacterial cells were re-suspended in PBS (pH 7.2, 0.01 mol/L) and counted by ultraviolet spectrophotometer at OD_{600}. Subsequently, 100 μL of bacterial suspension (1×10^7 CFU/mL) was uniformly dropped onto the nanofibrous matrices which were cut into small circular discs with a diameter around 16 cm, and then placed in a 100 mL aseptic seal bottle and incubated for 18 h at 37 °C. After this, 10 mL PBS was added to each bottle and the samples were full shaken in order to detach the bacterial from the matrices. The eluents were then gradient diluted (10^{-1}, 10^{-2} and 10^{-3} respectively), and 100 μL of the diluent was spread onto the solidified nutrient agar medium and incubated at 37 °C for 24 h. Finally, the number of colony was counted and the antimicrobial activity of

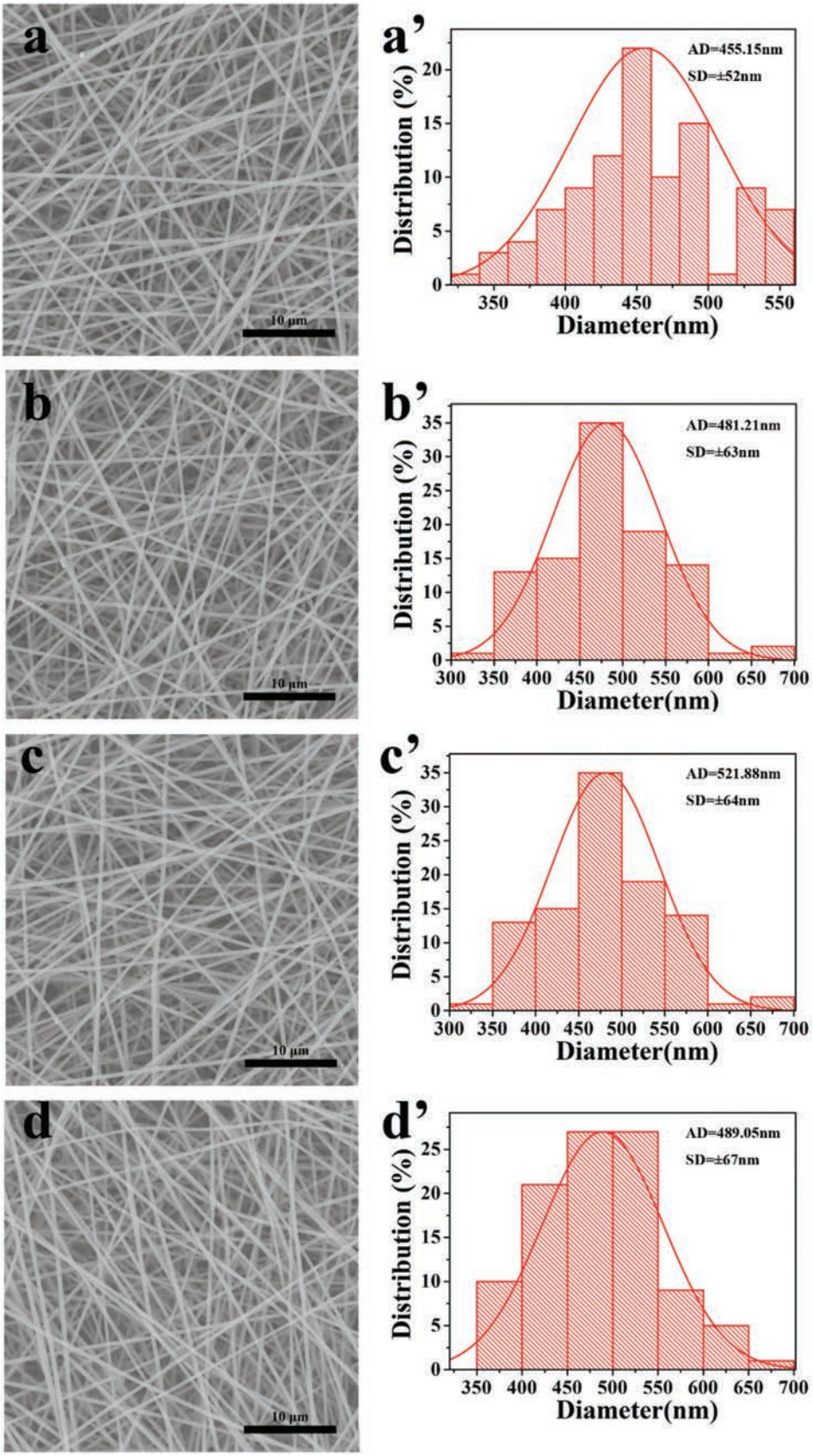

Figure 1. **SEM images and diameter distributions of the nanofibers. (a and a′) SF; (b and b′) HPRP-A2 (0.002%)/SF; (c and c′) HPRP-A2 (0.004%)/SF; (d and d′) HPRP-A2 (0.01%)/SF.**

the samples can be calculated by the following equation.[28]

$$\text{Bacterial inhibition} = \left(\frac{A-B}{A}\right) \times 100\%$$

(where A and B are mean numbers of the bacteria on the samples without and with the nanofibrous matrices, respectively).

In Vivo Wound Healing Test

ICR mice of 6–8 weeks old were injected with 100 μL sodium pentobarbital at a concentration of 1%, then a 10 mm circular wound was created on the dorsal region. Subsequently, the nanofibrous matrices or wound plaster (used as positive control) were placed on the wound site, and the mice received no treatment as negative control. On days 4, 7, 11 and 15, the change in wound area was photographed and measured using Image J analysis software. Each sample was tested on three mice. The wound healing effect is expressed as the percentage of wound size that remained exposed. The percentage of the wound size was obtained via comparing the wound size on days 4, 7, 11, or 15 with that on day 0.

$$\text{wound size } (\%) = W_{4,7,11,15}/W_0 \times 100\%$$

(Where $W_{(4,7,11,15)}$ and W_0 represent the exposed areas of the wounds on 0 and 4, 7, 11, and 15 day time point, respectively).

Statistical Analysis

The experiments were conducted at least triplicate and the data were expressed as means ± standard deviation (SD).

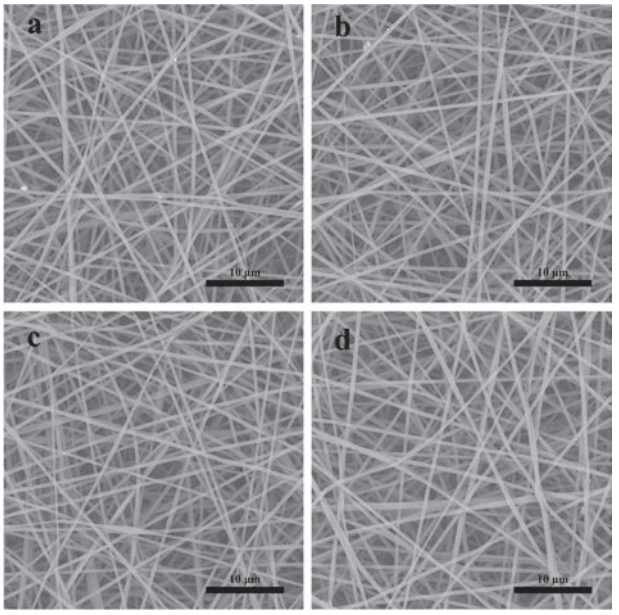

Figure 2. SEM images of the fibrous matrices treated with 75% (v/v) ethanol vapor. (a) SF; (b) HPRP-A2 (0.002%)/SF; (c) HPRP-A2 (0.004%)/SF; (d): HPRP-A2 (0.01%)/SF.

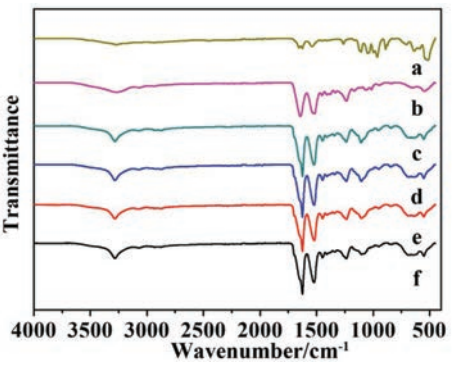

Figure 3. FTIR spectra of the nanofibers (a: HPRP-A2; b: SF nanofibers without post treatment; c: SF nanofibers; d: HPRP-A2 (0.002%)/SF nanofibers; e: HPRP-A2 (0.004%)/SF nanofibers; f: HPRP-A2 (0.01%)/SF nanofibers; samples of c-f were treated with 75% (v/v) ethanol vapor).

The error bars represent the standard deviation in the figures. Statistical analysis was performed by one-way ANOVA using Origin 8.0 (Origin Lab, USA). In all statistical comparisons, values of $P < 0.05$ were considered statistically significant.

RESULTS AND DISCUSSION

Surface Morphology of Nanofibrous Matrices

According to our previous study,[2] the concentration of aqueous SF solution in the electrospinning was set as 20% (w/v) and 2% (w/v) PEO was added to enhance the spinnability of the SF solution. In this work, different amounts of HPRP-A2 were added to the electrospinning solution, respectively. As shown in Figure 1, the composite nanofibers have a round and smooth morphology with an average diameter about 500 nm. The incorporation of HPRP-A2 did not significantly change the morphology and diameter of SF nanofibers. In order to improve the water-resistance ability of nanofibrous matrices, the products were treated with 75% ethanol vapor for 24 h. The results

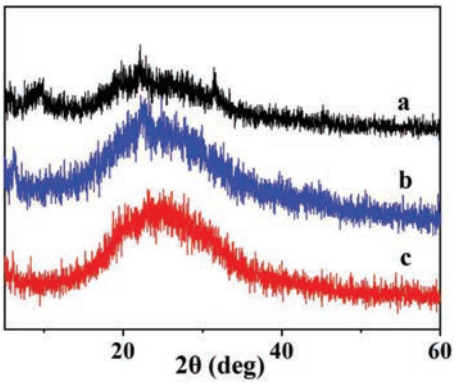

Figure 4. Wide-angle XRD profiles of the nanofibers after treatment with 75% (v/v) ethanol vapor (a: HPRP-A2; b: SF and c: HPRP-A2/SF).

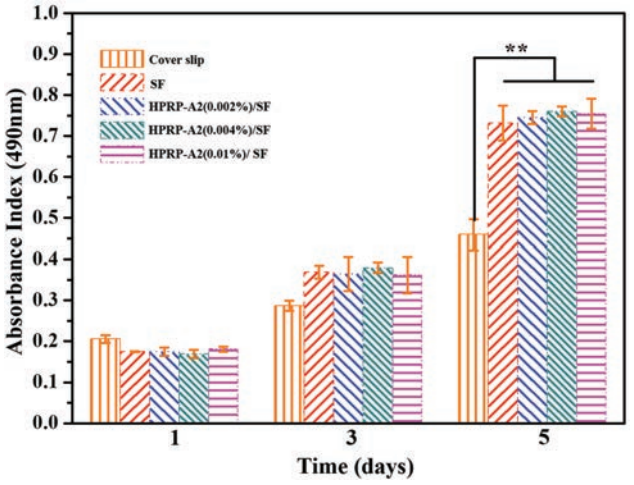

Figure 5. **The viability of cells grown on the cover slips and different matrices (** $^{**}P < 0.01$**).**

indicated the nanofibers remained a good morphology after the treatment with ethanol vapor (Fig. 2).

Secondary Structure of Nanofibrous Matrices

ATR-FTIR spectroscopy was used to characterize the changes of the surface chemical compositions of nanofibrous matrices after ethanol vapour treatment. As shown in Figure 3(b), the untreated SF nanofibrous matrices have characteristic absorption bands of amide I (C–O stretching vibration), amide II (C–N stretching vibration and N–H bending vibration) and amide III (C–N stretching vibration) at 1645 cm^{-1}, 1515 cm^{-1}, and 1230 cm^{-1}, respectively.[30, 31] After treatment with ethanol vapour, the above characteristic absorption peaks of SF shifted to 1629 cm^{-1}, 1520 cm^{-1} and 1236 cm^{-1} respectively, suggesting a conformation change from silk I to silk II.[2] While HPRP-A2 shows characteristic absorption peaks at 1623 cm^{-1} (amide I) and 1537 cm^{-1} (amide II), which represents a predominant α-helical structure.[32] With increase of HPRP-A2 content (Figs. 3(d–f)), the bands at 1629 cm^{-1} and 1520 cm^{-1} shifted to higher wave numbers in the HPRP-A2/SF nanofibrous matrices, indicating that HPRP-A2 was successfully incorporated into the nanofibrous matrices.

XRD was used to detect effect of HPRP-A2 on the crystallinity of SF nanofibers. Polymers with higher crystallinity have sharper and stronger XRD peaks, while relatively weak and wide range peaks indicate the amorphous regions in polymers. As shown in Figure 4, HPRP-A2 has multiple diffraction peaks at $2\theta = 9.873°$, 18.904°, 22.099°, 25.797° and 31.460°, and SF nanofibers have a diffraction peak at $2\theta = 22.601°$, while the diffraction peak of HPRP-A2/SF composite nanofibers is seen at $2\theta = 24.615°$, wider than that of SF nanofibers, suggesting some strong interaction occurred between SF and HPRP-A2 molecule in the blends. These data indicate that the incorporation of HPRP-A2 changes the phase structure of SF nanofibers during the electrospinning and reduced the crystallinity of the SF nanofibers.

Cytocompatibility of Nanofibrous Matrices

To investigate the cytocompatibility of composite nanofibrous matrices, the viability of L929 cells cultured on the matrices was analyzed by MTT assay. As shown in Figure 5, the cells cultured on SF nanofibrous matrices have higher viability than ones on cover slips, especially after a longer period of culture (3 and 5 days). There is no difference between pure SF nanofibrous matrices and the composite nanofibrous matrices loading different amounts

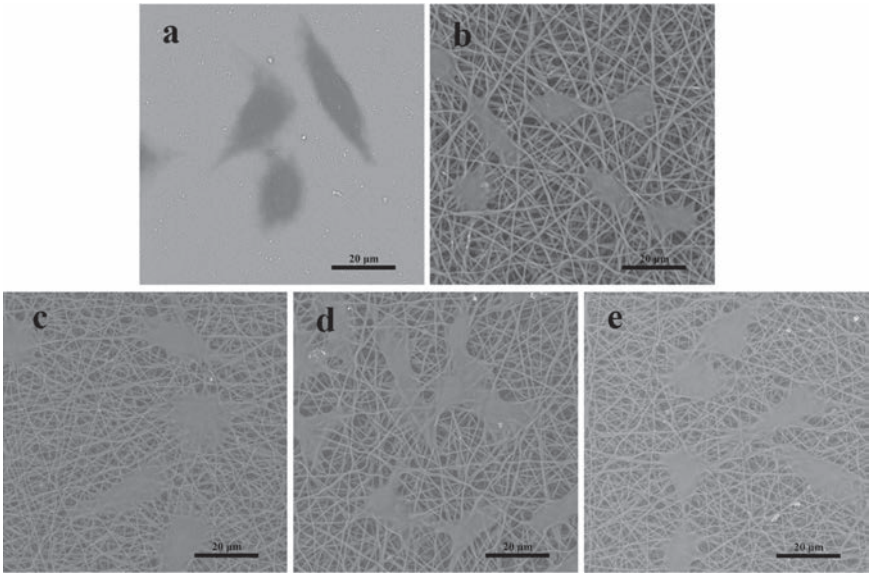

Figure 6. **SEM images of L929 cells grown on different substrates (a: Cover slips; b: SF nanofibrous matrices; c: HPRP-A2 (0.002%)/SF nanofibrous matrices; d: HPRP-A2 (0.004%)/SF nanofibrous matrices; e: HPRP-A2 (0.01%)/SF nanofibrous matrices).**

of HPRP-A2, indicating that the incorporation of HPRP-A2 does not adversely affect the biocompatibility of SF nanofibrous matrices. These data are consistent with those from fluorescence microscopy where more spindle-shaped cells are seen on nanofibrous matrices compared to cover slips (Fig. 7).

To further confirm the cytocompatibility of composite nanofibrous matrices, the morphology of L929 cells cultured on the nanofibrous matrices was observed by SEM. As shown in Figure 6, cells on both cover slips and nanofibrous matrices show a good morphology. Obviously, cells on both the neat and HPRP-A2 loaded SF nanofibrous matrices spread better and cell-cell and cell-matrix interactions are seen clearly, which is beneficial to signal transduction between cells and matrices.[33] These results demonstrate that the incorporation of HPRP-A2 has no negative effect on biocompatibility of SF nanofibrous matrices.

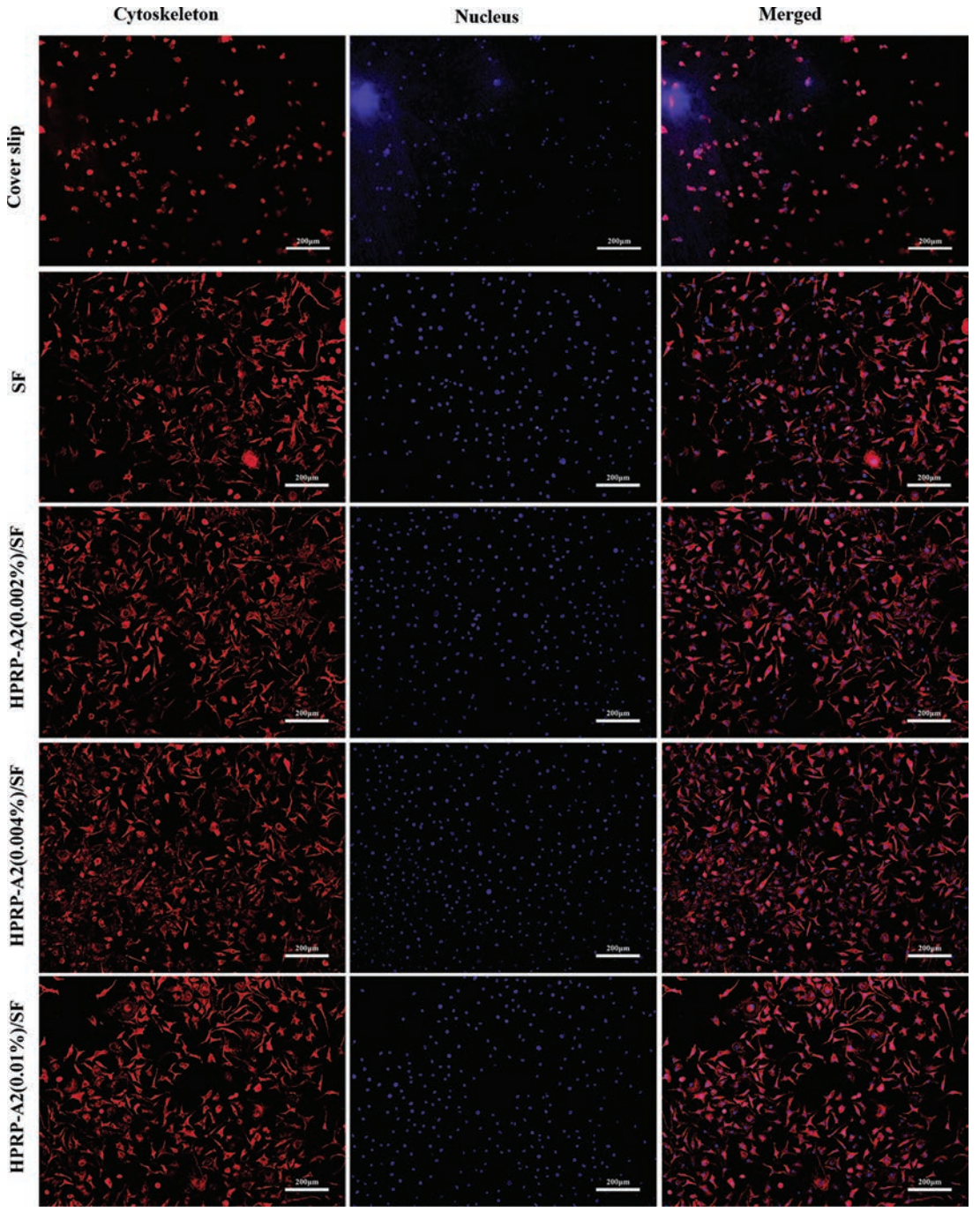

Figure 7. **Fluorescence microscopy images of L929 cells cultured on cover slips or SF nanofibrous matrices.**

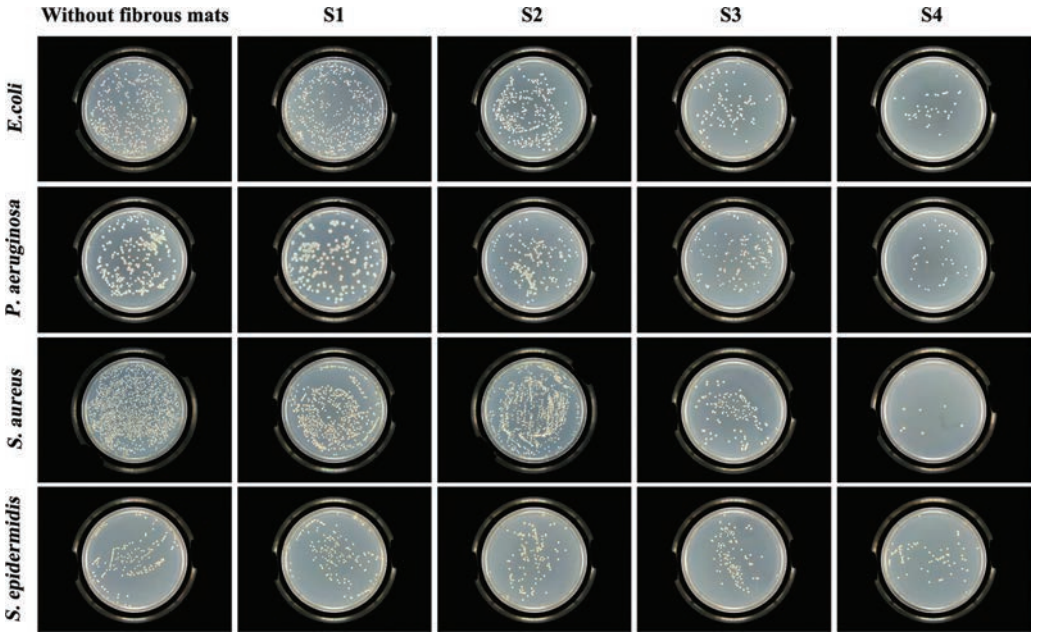

Figure 8. **Images of the bacteria colony detected after incubation for 24 hours (S1, S2, S3 and S4 represent SF nanofibrous matrices, HPRP-A2 (0.002%)/SF nanofibrous matrices, HPRP-A2 (0.004%)/SF nanofibrous matrices and HPRP-A2 (0.01%)/SF nanofibrous matrices, respectively).**

Antibacterial Activity of Nanofibrous Matrices

Antibacterial activity of the nanofibrous matrices was investigated using AATCC Quantitative Test Method 100-1999 against both Gram-negative bacteria (*E. coli* and *P. aeruginosa*) and Gram-positive bacteria (*S. aureus* and *S. epidermidis*). As shown in Figures 8 and 9, the SF nanofibrous matrices without loading HPRP-A2 show a negligible antibacterial effect. While the HPRP-A2 (0.002%)/SF, HPRP-A2 (0.004%)/SF and HPRP-A2 (0.01%)/SF nanofibrous matrices demonstrate a high

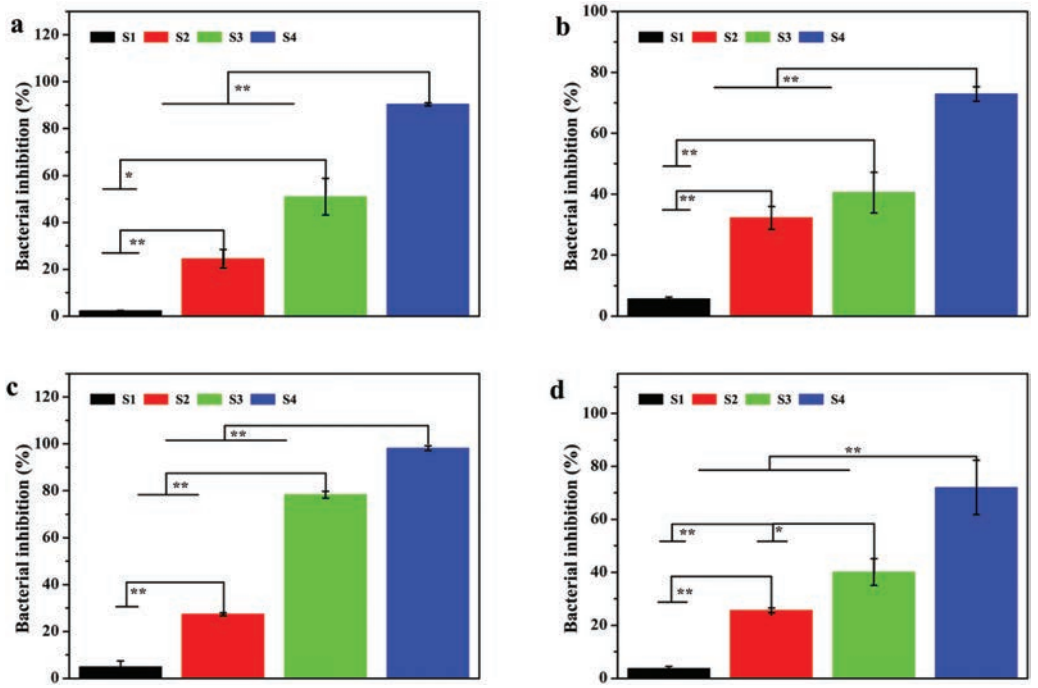

Figure 9. **Bacterial inhibition rates of different nanofibrous matrices (a: *E. coli*; b: *P. aeruginosa*; c: *S. aureus*; d: *S. epidermidis*; S1, S2, S3 and S4 represent SF nanofibrous matrices, HPRP-A2 (0.002%)/SF nanofibrous matrices, HPRP-A2 (0.004%)/SF nanofibrous matrices and HPRP-A2 (0.01%)/SF nanofibrous matrices, respectively).**

antibacterial capacity with antibacterial rates against *E. coli* (*P. aeruginosa*, *S. aureus* and *S. epidermidis*) for 24.2% (32.24%, 27.33%, 25.65%), 50.91% (40.54%, 78.35%, 40.06%) and 90.39% (72.93%, 98.19%, 72.05%), respectively (Figs. 8, 9(b–d)). Clearly, the bacterial inhibition efficacy of composite nanofibrous matrices significantly increases with the increase of HPRP-A2 content. Specifically, the HPRP-A2 (0.01%)/SF nanofibrous matrices show a strong inhibition against both Gram-positive and Gram-negative bacteria, indicating the antibacterial activity of HPRP-A2 was not significantly affected during the preparation of composite matrices. These findings indicate that the HPRP-A2 (0.01%)/SF nanofibrous matrices combine both the powerful antibacterial ability of HPRP-A2 and the excellent biocompatibility of SF well.

The emergence of resistant bacteria due to the abuse of traditional antibiotics has become one of serious threats to human health.[11, 12] A good strategy for this is to find alternates of antibiotics. The most commonly-used antibacterial substance in biomaterials is silver ion.[13, 34] However, silver ion has evident cytotoxicity.[13, 14] Copper ion is another heavy metal that has been reported to have good antibacterial activity.[36–38] Although copper is one of the essential trace elements in human body, excessive accumulation of copper ions can cause serious poisoning reactions.[39] Potential toxicity risks limit the application of silver and copper ions in biomedical field. Recently, the AMPs have attracted great attention for their outstanding antimicrobial ability.[15, 16] Unlike antibiotics, the AMPs kill bacteria by physical mechanisms, which makes them less likely to cause resistant bacteria.[10, 19] Therefore, the AMPs have been regarded as good alternatives to antibiotics. As one of the reported AMPs, HPRP-A2 has both excellent antimicrobial activity and stability.[12, 21] Here, we demonstrated that the HPRP-A2 incorporated into SF nanofibers via electrospinning still retains good antibacterial activity.

Wound Healing Effect of the Nanofibrous Matrices

The nanofibrous matrices and Wound Plaster (used as positive control) were applied on the wound area. Photographs of the wound area of different groups were taken on 4, 7, 11, and 15 day to check the change in the wound size (Fig. 10(a)). To determine the wound healing effects of the different materials, the percentage of the wound size that remained exposed was obtained via comparing the wound size on specific time point with that on initial time (Fig. 10(b)). As shown in Figure 10, the wound size of the mice treated with the tested matrices or Wound Plaster was much smaller than the negative control ($p < 0.05$), which indicated that both the neat SF and HPRP-A2/SF nanofibrous matrices are helpful to wound healing. The results also confirmed the beneficial of SF nanofibrous matrices to skin and wound healing as reported in our previous studies.[2, 25–28] Moreover, the addition of HPRP-A2 significantly improved

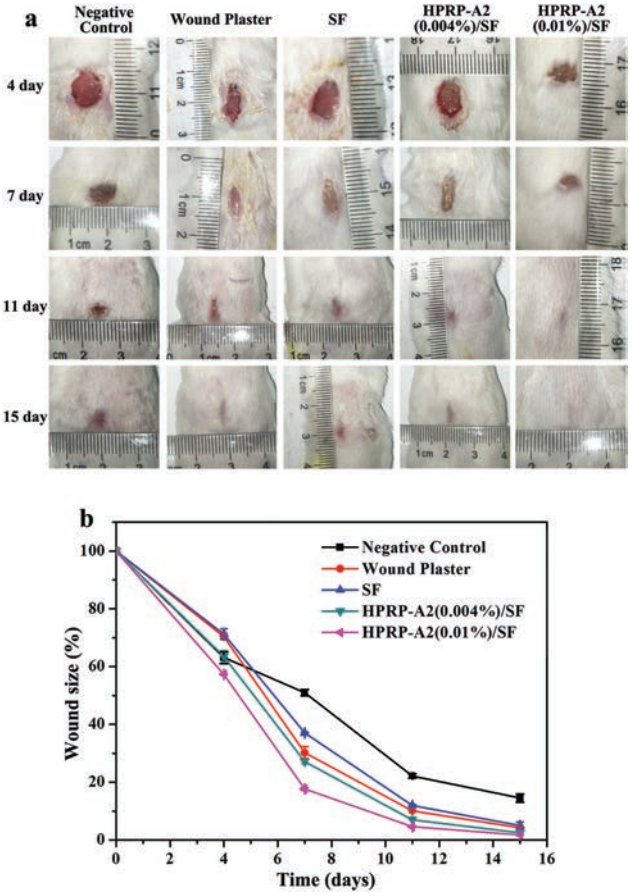

Figure 10. Photographic images of the extent of wound healing (a) and graphical illustration of the size change of the wound area (b) under different treatment.

the wound healing rate of SF nanofibrous matrices ($p < 0.05$). Specifically, the HPRP-A2 (0.01%)/SF composites treated wound showed a much better healing effect than that of the Wound Plaster ($p < 0.01$). In our previous study, the honey-loaded SF matrices also showed good performance on antibacterial activity and wound healing.[2] In together, our studies confirm the extreme importance of anti-infection in wound healing. Considering the facile technique and green process, HPRP-A2/SF nanofibrous matrices could be a promising candidate for practical applications such as antibacterial management and wound healing.

CONCLUSIONS

In the present study, a novel SF nanofibrous matrices loading HPRP-A2 were successfully fabricated via a green electrospinning. The incorporation of HPRP-A2 does not significantly change both the morphology and biocompatibility of SF nanofibrous matrices. Furthermore, the composite matrices showed an impressive antimicrobial activity against both Gram-positive and Gram-negative bacteria. *In vivo* wound healing assay

indicated that HPRP-A2/SF nanofibrous matrices can significantly accelerate wound healing. Specifically, the HPRP-A2(0.01%)/SF nanofibrous matrices inherited both the outstanding properties of HPRP-A2 and SF, with an excellent biocompatibility and antibacterial capacity, as well as a good effect on enhancing wound healing, suggesting a promising potential for this material serving in wound healing and antibacterial management.

Acknowledgments: This work was supported by the National Key Research and Development Program of China (2018YFB1105602), National Key Science and Technology Project (2017ZX09309001), Shanghai Science and Technology Committee Project (18490740400), Open Foundation of Key Laboratory of Science and Technology of Eco-Textile (Eco-KF-201612), Opening project of Zhejiang provincial preponderant and characteristic subject of key university (traditional Chinese pharmacology), Zhejiang Chinese Medical University (ZYAOX2018008), and the Innovation Foundation of Donghua University (EG2018018).

REFERENCES

1. Y. Wang, C. Fu, Z. Wu, L. Chen, X. Chen, Y. Wei, and P. Zhang, A chitin film containing basic fibroblast growth factor with a chitin-binding domain as wound dressings. *Carbohydr Polym.* 174, 723 **(2017)**.
2. X. Yang, L. Fan, L. Ma, Y. Wang, S. Lin, F. Yu, X. Pan, G. Luo, D. Zhang, and H. Wang, Green electrospun Manuka honey/silk fibroin fibrous matrices as potential wound dressing. *Mater. Des.* 119, 76 **(2017)**.
3. J. Xiao, S. Chen, J. Yi, H. Zhang, and G. A. Ameer, A cooperative copper metal-organic framework-hydrogel system improves wound healing in diabetes. *Adv Funct Mater.* 27, 1 **(2017)**.
4. T. Hakkarainen, R. Koivuniemi, M. Kosonen, C. Escobedo-Lucea, A. Sanz-Garcia, J. Vuola, J. Valtonen, P. Tammela, A. Makitie, K. Luukko, M. Yliperttula, and H. Kavola, Nanofibrillar cellulose wound dressing in skin graft donor site treatment. *J. Control Release* 244, 292 **(2016)**.
5. M. Naseri-Nosar, S. Farzamfar, H. Sahrapeyma, S. Ghorbani, F. Bastami, A. Vaez, and M. Salehi, Cerium oxide nanoparticle-containing poly(epsilon-caprolactone)/gelatin electrospun film as a potential wound dressing material: *In vitro* and *in vivo* evaluation. *Mater. Sci. Eng. C Mater. Biol. Appl.* 81, 366 **(2017)**.
6. A. R. Unnithan, G. Gnanasekaran, Y. Sathishkumar, Y. S. Lee, and C. S. Kim, Electrospun antibacterial polyurethane-cellulose acetate-zein composite mats for wound dressing. *Carbohydr. Polym.* 102, 884 **(2014)**.
7. H. Chen, X. Xing, H. Tan, Y. Jia, T. Zhou, Y. Chen, Z. Ling, and X. Hu, Covalently antibacterial alginate-chitosan hydrogel dressing integrated gelatin microspheres containing tetracycline hydrochloride for wound healing. *Mater. Sci. Eng. C Mater. Biol. Appl.* 70, 287 **(2017)**.
8. Y. Ma, L. Xin, H. Tan, M. Fan, J. Li, Y. Jia, Z. Ling, Y. Chen, and X. Hu, Chitosan membrane dressings toughened by glycerol to load antibacterial drugs for wound healing. *Mater. Sci. Eng. C Mater. Biol. Appl.* 81, 522 **(2017)**.
9. S. Saghazadeh, C. Rinoldi, M. Schot, S. S. Kashaf, F. Sharifi, E. Jalilian, K. Nuutila, G. Giatsidis, P. Mostafalu, H. Derakhshandeh, K. Yue, W. Swieszkowski, A. Memic, A. Tamayol, and A. Khademhosseini, Drug delivery systems and materials for wound healing applications. *Adv. Drug Deliv. Rev.* 127, 138 **(2018)**.
10. W. Y. Chen, H. Y. Chang, J. K. Lu, Y. C. Huang, S. G. Harroun, Y. T. Tseng, Y. J. Li, C. C. Huang, and H. T. Chang, Self-assembly of antimicrobial peptides on gold nanodots: Against multidrug-resistant bacteria and wound-healing application. *Adv. Funct. Mater.* 25, 7189 **(2015)**.
11. H. Nikaido, Multidrug resistance in bacteria. *Annual Review of Biochemistry* 78, 119 **(2009)**.
12. Q. Feng, Y. Huang, M. Chen, G. Li, and Y. Chen, Functional synergy of alpha-helical antimicrobial peptides and traditional antibiotics against Gram-negative and Gram-positive bacteria *in vitro* and *in vivo*. *European Journal of Clinical Microbiology and Infectious Diseases* 34, 197 **(2015)**.
13. B. S. Atiyeh, M. Costagliola, S. N. Hayek, and S. A. Dibo, Effect of silver on burn wound infection control and healing: Review of the literature. *Burns* 33, 139 **(2007)**.
14. J. W. Loh, G. Yeoh, M. Saunders, and L. Y. Lim, Uptake and cytotoxicity of chitosan nanoparticles in human liver cells. *Toxicol. Appl. Pharmacol.* 249, 148 **(2010)**.
15. H. N. Huang, C. Y. Pan, Y. L. Chan, J. Y. Chen, and C. J. Wu, Use of the antimicrobial peptide pardaxin (GE33) to protect against methicillin-resistant *Staphylococcus aureus* infection in mice with skin injuries. *Antimicrob Agents Chemother* 58, 1538 **(2014)**.
16. K. Hilpert, M. Elliott, H. Jenssen, J. Kindrachuk, C. D. Fjell, J. Korner, D. F. Winkler, L. L. Weaver, P. Henklein, A. S. Ulrich, S. H. Chiang, S. W. Farmer, N. Pante, R. Volkmer, and R. E. Hancock, Screening and characterization of surface-tethered cationic peptides for antimicrobial activity. *Chem. Biol.* 16, 58 **(2009)**.
17. L. Bai, L. Zhu, S. Min, L. Liu, Y. Cai, and J. Yao, Surface modification and properties of bombyx mori silk fibroin films by antimicrobial peptide. *Appl. Surf. Sci.* 254, 2988 **(2008)**.
18. D. W. Song, S. H. Kim, H. H. Kim, K. H. Lee, C. S. Ki, and Y. H. Park, Multi-biofunction of antimicrobial peptide-immobilized silk fibroin nanofiber membrane: Implications for wound healing, *Acta Biomater.* 39, 146 **(2016)**.
19. H. P. Felgueiras and M. T. P. Amorim, Functionalization of electrospun polymeric wound dressings with antimicrobial peptides. *Colloids Surf. B Biointerfaces* 156, 133 **(2017)**.
20. K. Putsep, C. I. Branden, H. G. Boman, and S. Normark, Antibacterial peptide from H-pylori. *Nature* 398, 671 **(1999)**.
21. L. Zhao, Y. Huang, S. Gao, Y. Cui, D. He, L. Wang, and Y. Chen, Comparison on effect of hydrophobicity on the antibacterial and antifungal activities of α-helical antimicrobial peptides. *Science China Chemistry* 56, 1307 **(2013)**.
22. L. Fan, J. L. Li, Z. Cai, and X. Wang, Creating biomimetic anisotropic architectures with co-aligned nanofibers and macrochannels by manipulating ice crystallization. *ACS Nano* 12, 5780 **(2018)**.
23. V. N. Chamundeswari, Y. J. Chuah, and S. C. J. Loo, Multidrug-eluting bi-layered microparticle-mesh scaffolds for musculoskeletal tissue regeneration. *Journal of Materials Chemistry B* 6, 3340 **(2018)**.
24. L. P. Fan, H. S. Wang, K. H. Zhang, C. L. He, Z. X. Cai, and X. M. Mo, Regenerated silk fibroin nanofibrous matrices treated with 75% ethanol vapor for tissue-engineering applications. *Journal of Biomaterials Science* 23, 497 **(2012)**.
25. L. P. Fan, Z. X. Cai, K. H. Zhang, F. Han, J. L. Li, C. L. He, X. M. Mo, X. G. Wang, and H. S. Wang, Green electrospun pantothenic acid/silk fibroin composite nanofibers: Fabrication, characterization and biological activity. *Colloids and Surfaces B-Biointerfaces* 117, 14 **(2014)**.
26. L. P. Fan, H. S. Wang, K. H. Zhang, Z. X. Cai, C. L. He, X. Y. Sheng, and X. M. Mo, Vitamin C-reinforcing silk fibroin nanofibrous matrices for skin care application. *Rsc Advances* 2, 4110 **(2012)**.
27. X. Sheng, L. Fan, C. He, K. Zhang, X. Mo, and H. Wang, Vitamin E-loaded silk fibroin nanofibrous mats fabricated by green process for skin care application. *Int. J. Biol. Macromol.* 56, 49 **(2013)**.
28. S. Lin, M. Chen, H. Jiang, L. Fan, B. Sun, F. Yu, X. Yang, X. Lou, C. He, and H. Wang, Green electrospun grape seed extract-loaded

silk fibroin nanofibrous mats with excellent cytocompatibility and antioxidant effect. *Colloids Surf. B Biointerfaces* 139, 156 **(2016)**.

29. X. Liu, T. Lin, Y. Gao, Z. Xu, C. Huang, G. Yao, L. Jiang, Y. Tang, and X. Wang, Antimicrobial electrospun nanofibers of cellulose acetate and polyester urethane composite for wound dressing. *J. Biomed. Mater. Res. B Appl. Biomater.* 100, 1556 **(2012)**.

30. X. Lv, Z. Li, S. Chen, M. Xie, J. Huang, X. Peng, R. Yang, H. Wang, Y. Xu, and C. Feng, Structural and functional evaluation of oxygenating keratin/silk fibroin scaffold and initial assessment of their potential for urethral tissue engineering. *Biomaterials* 84, 99 **(2016)**.

31. Y. H. Shan, L. H. Peng, X. Liu, X. Chen, J. Xiong, and J. Q. Gao, Silk fibroin/gelatin electrospun nanofibrous dressing functionalized with astragaloside IV induces healing and anti-scar effects on burn wound. *Int. J. Pharm.* 479, 291 **(2015)**.

32. E. Gazit, I. R. Miller, P. C. Biggin, M. S. P. Sansom, and Y. Shai, Structure and orientation of the mammalian antibacterial peptide cecropin P1 within phospholipid membranes. *J. Mol. Biol.* 258, 860 **(1996)**.

33. D. H. Roh, S. Y. Kang, J. Y. Kim, Y. B. Kwon, H. Y. Kweon, K. G. Lee, Y. H. Park, R. M. Baek, C. Y. Heo, J. Choe, and J. H. Lee, Wound healing effect of silk fibroin/alginate-blended sponge in full thickness skin defect of rat. *J. Mater. Sci.-Mater. Med.* 17, 547 **(2006)**.

34. Q. Li, F. Lu, G. Zhou, K. Yu, B. Lu, Y. Xiao, F. Dai, D. Wu, and G. Lan, Silver inlaid with gold nanoparticle/chitosan wound dressing enhances antibacterial activity and porosity, and promotes wound healing. *Biomacromolecules* 18, 3766 **(2017)**.

35. S. Zhao, L. Li, H. Wang, Y. Zhang, X. Cheng, N. Zhou, M. N. Rahaman, Z. Liu, W. Huang, and C. Zhang, Wound dressings composed of copper-doped borate bioactive glass microfibers stimulate angiogenesis and heal full-thickness skin defects in a rodent model. *Biomaterials* 53, 379 **(2015)**.

36. S. Zhao, H. Wang, Y. Zhang, W. Huang, M. Rahaman, Z. Liu, D. Wang, and C. Zhang, Copper-doped borosilicate bioactive glass scaffolds with improved angiogenic and osteogenic capacity for repairing osseous defects. *Acta Biomaterialia* 14, 185 **(2015)**.

37. J. Li, D. Zhai, F. Lv, Q. Yu, H. Ma, J. Yin, Z. Yi, M. Liu, J. Chang, and C. Wu, Preparation of copper-containing bioactive glass/eggshell membrane nanocomposites for improving angiogenesis, antibacterial activity and wound healing. *Acta Biomater.* 36, 254 **(2016)**.

38. L. Guo, I. Panderi, D. D. Yan, K. Szulak, Y. Li, Y. T. Chen, H. Ma, D. B. Niesen, N. Seeram, and A. Ahmed, A comparative study of hollow copper sulfide nanoparticles and hollow gold nanospheres on degradability and toxicity. *Acs Nano* 7, 8780 **(2013)**.